β phase and γ-β metal-insulator transition in multiferroic $BiFeO_3$

R. Palai,[1] R. S. Katiyar,[1] H. Schmid,[2] P. Tissot,[2] S. J. Clark,[3] J. Robertson,[4] S. A. T. Redfern,[5] G. Catalan,[5] and J. F. Scott[5]
[1]*Department of Physics and Institute for Functional Nanomaterials, University of Puerto Rico, San Juan, Puerto Rico 00931-3343, USA*
[2]*Department of Inorganic, Analytical and Applied Chemistry, University of Geneva, CH-1211 Geneva 4, Switzerland*
[3]*Department of Physics, Durham University, Durham DH1 3LE, United Kingdom*
[4]*Department of Engineering, University of Cambridge, Cambridge CB2 1PZ, United Kingdom*
[5]*Department of Earth Science, University of Cambridge, Cambridge CB2 3EQ, United Kingdom*
(Received 17 August 2007; revised manuscript received 17 October 2007; published 28 January 2008)

We report on extensive experimental studies on thin film, single crystal, and ceramics of multiferroic bismuth ferrite $BiFeO_3$ using differential thermal analysis, high-temperature polarized light microscopy, high-temperature and polarized Raman spectroscopy, high-temperature x-ray diffraction, dc conductivity, optical absorption and reflectivity, and domain imaging, and show that epitaxial (001) thin films of $BiFeO_3$ are clearly monoclinic at room temperature, in agreement with recent synchrotron studies but in disagreement with all other earlier reported results. We report an *orthorhombic* order-disorder β phase between 820 and 925 (± 5) °C, and establish the existence range of the cubic γ phase between 925 (± 5) and 933 (± 5) °C, contrary to all recent reports. We also report the refined Bi_2O_3-Fe_2O_3 phase diagram. The phase transition sequence rhombohedral-orthorhombic-cubic in bulk [monoclinic-orthorhombic-cubic in (001)$BiFeO_3$ thin film] differs distinctly from that of $BaTiO_3$. The transition to the cubic γ phase causes an abrupt collapse of the band gap toward zero (insulator-metal transition) at the orthorhombic-cubic β-γ transition around 930 °C. Our band structure models, high-temperature dc resistivity, and light absorption and reflectivity measurements are consistent with this metal-insulator transition.

DOI: 10.1103/PhysRevB.77.014110 PACS number(s): 64.70.K−, 71.30.+h, 78.30.−j, 77.55.+f

I. INTRODUCTION

Magnetoelectric (ME) multiferroics[1] are technologically and scientifically promising because of their potential applications in data storage, spin valves, spintronics, quantum electromagnets, microelectronic devices, etc.[2–4] Ferroelectricity originates from off-center structural distortions (d^0 electrons) and magnetism is involved with local spins (d^n electrons), which limit the presence of off-center structural distortion.[5] These two are quite complementary phenomena, but coexist in certain unusual multiferroic materials. $BiFeO_3$ (BFO) is one of the most widely studied multiferroic material because of its interesting ME properties, i.e., ferroelectricity with high Curie temperature[6] ($T_C \approx 810-830$ °C) and antiferromagnetic properties below $T_N \approx 370$ °C.[6,7] The bulk BFO single crystal shows rhombohedral ($a=5.58$ Å and $\alpha=89.5$ °) crystal structure at room temperature (RT) with the space group $R3c$ and G-type antiferromagnetism.[7,8] If BFO were an ordinary antiferromagnet, the magnetic space group would be expected to be $R3c$ (Heesch-Shubnikov point group $3m$), however, the antiferromagnetic structure is incommensurate (IC) with a cycloidal modulation.[9] Whereas this modulation suppresses the linear ME effect, the bilinear ME effect survives, simulating a paramagnetic point group $3m1'$ for the IC phase.[10] The structure and properties of bulk BFO have been studied extensively.[6–8,11,12]

Early values of polarization were very low due to sample quality, but, recently, $P_r=40-50$ $\mu C/cm^2$ was found in bulk by several different groups.[13,14] However, recently even, about $P_r=100$ $\mu C/cm^2$ was measured on single crystals, matching the high values of spontaneous polarization achieved in thin films (see below).[15] Thus, these well insulating single crystals, although still relatively small, yielding a high, filmlike spontaneous polarization, represent a certain progress relative to the fernlike dendritic single crystals[16] (Fig. 1) and to the dendritic polar single domain crystals with (100)-pseudo-cubic habitus.[8,17] Thus, the growth of large, high quality, and defect-free single crystals with low leakage still remains a challenge.

It has been found that thin films of BFO grown on $SrTiO_3$ (STO) substrates show very high values of P_r [~55, 86, and 98 $\mu C/cm^2$ for the (001), (101), and (111) BFO films, respectively] and magnetization ($M_r \sim 150$ emu/cc).[2,18,19] (Very recently, Yun *et al.*[20] have claimed P_r of 250 $\mu C/cm^2$ for the polycrystalline BFO films grown on $Pt/TiO_2/SiO_2/Si$ substrates, but this is probably an artifact due to leakage and charge injection.) This makes BFO as one of the potential materials for novel device applications, although the mechanism(s) behind the huge polarization claimed by some groups is not yet fully understood. Some experimental results[2,18] and theoretical reports[21] suggest that the epitaxial strain might be the cause of such high value of P_r and M_r. However, a recent study showed that the epitaxial strain does not enhance M_r in BFO thin films.[22] It is believed that the heteroepitaxy induces significant and important structural changes in BFO thin films, which may lead to higher values for P_r than found in single crystals.

There are some controversies in literature about the crystal structure of (001) epitaxial thin films. There have been several reports claiming tetragonal,[2,23] rhombohedral,[19,24] and monoclinic[25] structure of (001) BFO films on STO substrates. Therefore, the sequence of transitions in layers is poorly understood, and there is no understanding of the overall physics of the phase transitions involved; more structural

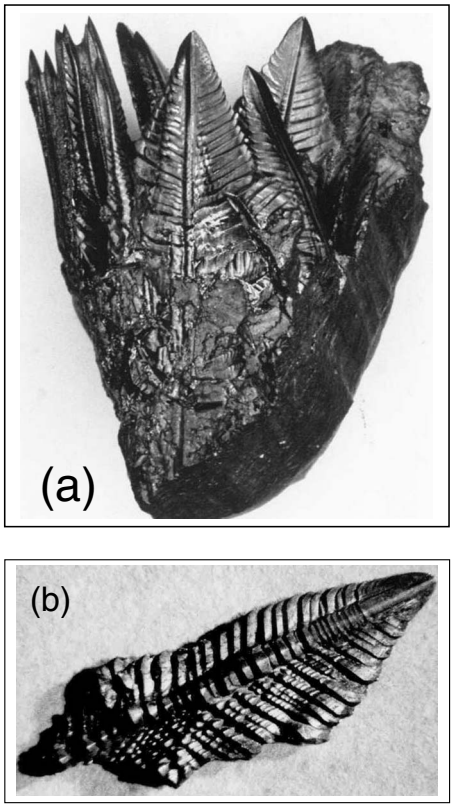

FIG. 1. As-grown dendrites of $BiFeO_3$: (a) bunch of leaves grown in a Pt crucible; (b) individual leaf, axis parallel to ⟨110⟩pc, plane of leaf parallel to (110)pc. The horizontal axis is ~2.5 and 1 cm in (a) and (b), respectively.

analyses of thin films are necessary for better understanding of engineered epitaxial and heterostructure BFO thin films. Here, we report that the BFO(001) thin films are clearly monoclinic, in agreement with synchrotron data but contrary to the bulklike rhombohedral and tetragonal structures reported earlier; the β phase is unambiguously *orthorhombic*, in disagreement with all other recent publications.

An extremely large and unexplained drop (40%) in the band-gap energy within the monoclinic phase as temperature is increased from 300 to 800 K implies a strong and unknown electron-phonon interaction. The concomitant lattice contraction in the cubic γ phase shows the cubic phase is *metallic* and the material has large negative thermal expansion, which is very rare (e.g., Zr-tungstate) and never found in perovskites. The existence of insulator-metal transition above magnetic ordered states implies that the metallic transition could only be due to lattice contraction. Although the phase sequence is different from that in $BaTiO_3$, the succession of order-disorder transitions resembles that in the eight-site model of Comes *et al.*[26]

ABO_3 oxide perovskites which are rhombohedral at low temperatures, such as $LaAlO_3$, $PrAlO_3$, or $NdAlO_3$,[27,28] have ferroelastic instabilities at the *A*-ion site that induce displacive phase transitions directly to cubic, but those which have *B*-site instabilities instead have order-disorder transitions to cubic that involve two or more steps. This has been successfully described[26,29] by an eight-site model in which the *B*-ion displacements are always locally toward a [111] axis, but thermally average via hopping over [111], $[\bar{1}11]$, $[1\bar{1}1]$, and $[11\bar{1}]$ to give orthorhombic, tetragonal, or cubic time- and space-global averages. In the present work, we show that this model may describe BFO, contrary to conventional wisdom[30] but in agreement with NMR, which shows some *B*-site disorder.[31]

II. EXPERIMENTAL DETAILS

BFO thin films of 300 nm thickness were grown by pulsed laser deposition (PLD) using a 248 nm KrF Lambda Physik laser. Films were grown on STO(100) substrates of area $(5\ \text{mm})^2$ with ~25 nm thick $SrRuO_3$ (SRO) buffer layer. The orientation, crystal structure, and phase purity of the films were examined using Siemens D5000 x-ray diffractometer. The Jobin Yvon T64000 micro-Raman microprobe system with Ar ion laser ($\lambda = 514.5$ nm) in backscattering geometry was used for polarized and temperature-dependent Raman scattering. The laser excitation power was 2.5 mW and the acquisition time was 10 min per spectrum. The high-temperature x-ray data were collected from powdered bulk material prepared by high energy ball milling using a Bruker D8-ADVANCE diffractometer with Cu radiation, Göbel mirror, and fast Vantec linear position sensitive detector. Scans from 20° to 80° 2θ were obtained every 15° from 40° to the decomposition point of BFO with an acquisition time of 8 min per pattern and a heating rate of 30 °C/min between scans. The differential thermal analysis (DTA) measurements on the Bi_2O_3-Fe_2O_3 phase diagram were performed with a Mettler TA 1 thermoanalyzer in nitrogen atmosphere with a heating rate of 500 °C/h up to 750 °C. Above that temperature, heating-cooling cycles with a rate of 120 °C/h were practiced. The sample and reference material weights were 0.2 g, contained in platinum crucibles. Whereas Bi_2O_3/Fe_2O_3 powder mixtures were used for determining the *liquidus* curve, the peritectic and eutectic horizontals, crushed fernlike dendritic single crystals (Fig. 1) served for the exact $BiFeO_3$ composition.[16] The DTA measurements of target materials of thin film were carried out in air with a heating rate of 5 °C/min up to 1000 °C using Shimadzu DTA-50 differential thermal analyzer. The crystal growth of the fernlike dendrites was performed in platinum crucibles, using the accelerated crucible rotation technique,[32] with a crucible content of about 90 g and a platinum crucible cover, welded tightly to the crucible, leaving only a central hole of 0.1 mm diameter. For example, for a Bi_2O_3/Fe_2O_3 mixture of 23 mol % Fe_2O_3, the following temperature program was used: rapid heating to 1000 °C, soaking at 1000 °C for 24 h, cooling at 3 °C/h to 960 °C, thereafter linearly at 0.36 °C/h to 800 °C, cutting off the crucible cover, pouring off the remaining flux, and final cooling in furnace. Maximal size of dendritic leaves: $14 \times 5 \times 1.5\ \text{mm}^3$.[16] The ferroelastic domain structure of the α phase of these leaflets is explained in Ref. 10.

III. RAMAN EFFECT IN α PHASE

The rhombohedral ($R3c$), tetragonal ($P4mm$),[2] and monoclinic[33] (Bb) structures of BFO give rise to 13, 8, and

TABLE I. Selection rules for the Raman active modes for rhombohedral (R), tetragonal (T), and monoclinic (M) crystal structures in different polarization configurations with total number of normal (N) Raman modes. The notation "⟨001⟩up" means unpolarized spectra along the pseudocubic ⟨001⟩ direction perpendicular to the substrate. The notation Z (along ⟨001⟩ direction) and $\bar{Z}$ are the directions of the incident and backscattered light, respectively.

Scattering geometry	$R(R3c)$ (C_{3v})	$T(P4mm)$ (C_{4v})	$M(Bb)$ (C_s)
N (Raman)	$4A_1+9E$	$3A_1+B_1+4E$	$13A'+14A''$
⟨001⟩up	$4A_1+9E$	$3A_1+B_1$	$13A'$
Z(XX)$\bar{Z}$	A_1 and E	A_1 and B_1	A'
Z(XY)$\bar{Z}$	E	No modes	A'
Y(ZZ)$\bar{Y}$	A_1	A_1	A'
Y(ZX)$\bar{Y}$	E	E	A''

27 distinct Raman-active modes, respectively, as listed in Table I. For the orthorhombic distortion in the β phase, as discussed below, the tetragonal entries will remain correct, with only a small splitting of the E modes.

The unpolarized (perpendicular to the ⟨001⟩ of the substrate) Raman spectra of STO substrate, SRO/STO, and BFO/SRO/STO at room temperature are given in Fig. 2(a). The comparison of the spectrum of BFO thin film with STO and SRO/STO spectra precludes any Raman contribution from the substrate and bottom electrode; to the contrary, we observed a dip (rather than a peak) at the STO strongest peak position. As is evident from the intensity comparison, all of these peaks were due to BFO normal modes of vibrations and none of them arose from the substrate. We have verified our results using target materials and single crystals, and also by growing (001)BFO films on different substrates.[34]

The lowest peak around 74 cm^{-1} in our spectra looks very asymmetric and the deconvolution with the phonon fitting showed [Fig. 2(b)] two peaks at 71.6 and 76.3 cm^{-1} with R^2 value of 99% (the percentage of variation in the observed and fitted values), while the STO peak appears at 79.8 cm^{-1}. A clear splitting has been observed at cryogenic temperature.[34]

The polarized Raman spectra for 300 nm thick (001)BFO thin film on the SRO/STO substrate and (100)STO single-crystal substrate at room temperature in the parallel, Z(XX)$\bar{Z}$, and perpendicular, Z(XY)$\bar{Z}$, polarization configurations are given in Fig. 3. The comparison of polarized Raman spectra again clearly implies that there is no Raman contribution from the substrate on the BFO spectra. The spectra of BFO thin film [Fig. 3(a)] revealed strong peaks at around 72, 76, 140, 172, 219, 261, 269, and 289 cm^{-1}, while weaker peaks were observed at around 352, 370, 406, 478, 529, 547, 609, 808, 946, and 1093 cm^{-1} including few second-order peaks. The existence of 13 well defined and identical peaks in both the Z(XX)$\bar{Z}$ and Z(XY)$\bar{Z}$ polarization configurations confirms the Raman selection rules for the *monoclinic* structure (see Table I) instead of tetragonal or rhombohedral as reported earlier.[19,23,24] This observation

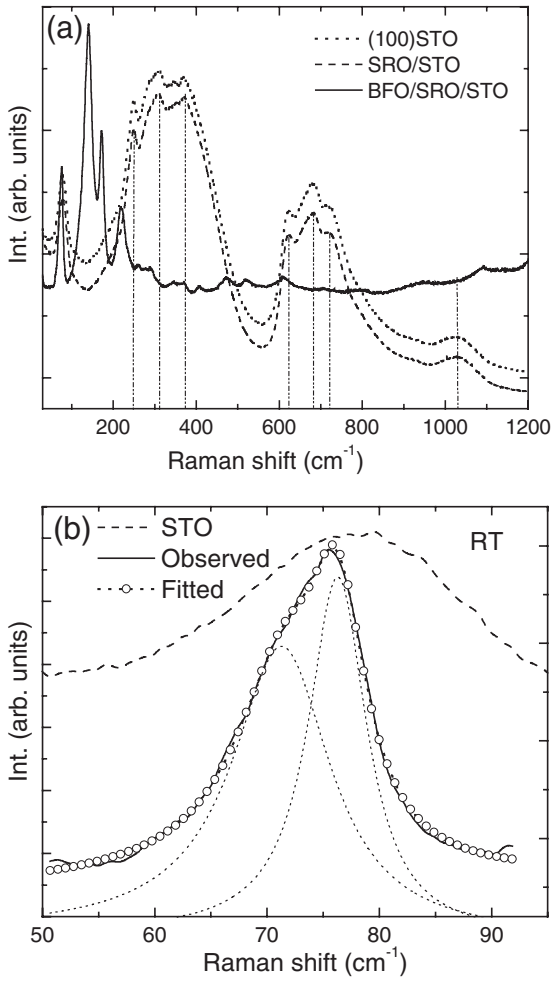

FIG. 2. (a) Comparison of unpolarized Raman spectra along ⟨001⟩ direction of (100)STO single crystal substrate, SRO/STO, and (001)BFO/SRO/STO thin film at room temperature. Lines are drawn as a guide for the eyes. (b) Deconvolution of the BFO peak around 74 cm^{-1} at RT shows the evolution of two peaks at 71.6 and 76.3 cm^{-1}. The "dotted line with empty circle" shows the fitting after the deconvolution of these two peaks. The STO(100) single-crystal substrate shows one peak at 79.8 cm^{-1} at RT, plotted for comparison.

verifies the very recent report of monoclinic structure for the epitaxial BFO films grown on (001)STO substrates by Xu *et al.*[25] studied via synchrotron radiation. We also investigated BFO thin films grown using different deposition techniques (PLD, metallo-organic chemical vapor deposition, and chemical solution deposition) on different single-crystal and textured substrates, and we found that films show monoclinic structure at room temperature down to 50 nm thickness. However, the single crystal clearly satisfies the Raman selection rules for the rhombohedral structure with $R3c$ symmetry. For a comparative study between epitaxial thin film and single crystal, refer to Ref. 34. Note that for ultrathin unrelaxed films, a tetragonal structure is possible, and our present work does not address these specimens. As the spectra along Y(ZZ)$\bar{Y}$ and Y(ZX)$\bar{Y}$ were heavily dominated by the scattering from the STO substrate, the contribution from the BFO film could not be separated.

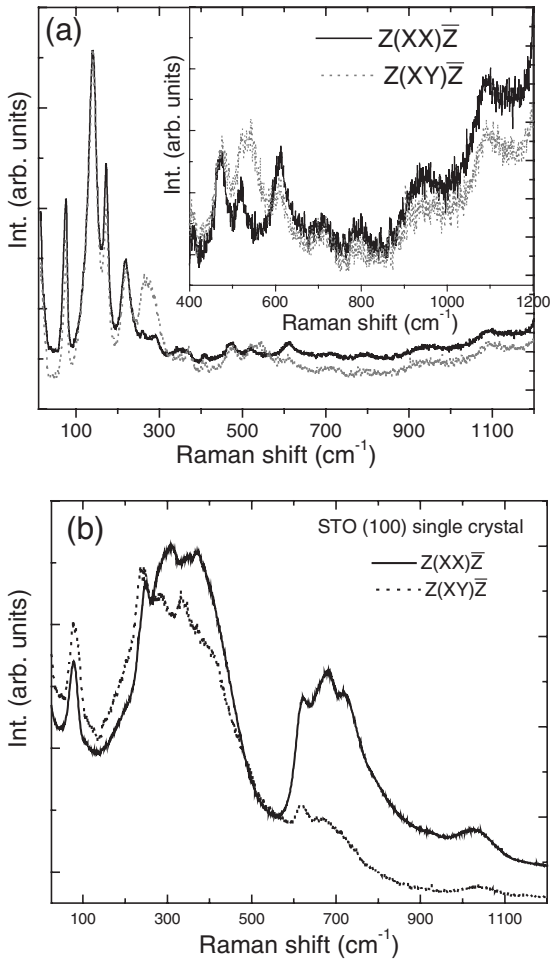

FIG. 3. (a) Polarized Raman spectra of (001)BFO thin film on SRO/STO in Z(XX)$\bar{Z}$ and Z(XY)$\bar{Z}$ scattering configurations. (b) Polarized Raman spectra of (100)STO substrate given for comparison.

If the theoretically derived, polar monoclinic space group[33] *Bb* describes, in fact, the ferromagnetism in monoclinically distorted thin films,[18] then the linear magnetoelectric effect is possible in principle, because all 13 ferromagnetic and/or ferroelectric Heesch-Shubnikov point groups are permitting the linear magnetoelectric effect.[35] The possible ferromagnetic subgroups of *Bb* of the nuclear structure are the ferromagnetic space groups *Bb* and *Bb′* (magnetic point groups *m* and *m′*, respectively).[33,36]

Figure 4 shows temperature-dependent Raman spectra of BFO thin film. A closer inspection of Raman spectra near the phase transition shows two noticeable changes: disappearance of all stronger peaks (72, 76, 140, 172, and 219 cm^{-1}) at ~820 °C with the appearance of a few new peaks, and complete disappearance of spectra around 950 °C. This temperature behavior implies that the BFO maintains its room-temperature structure up to ~820 °C, indicating the ferroelectric-ferroelectric (FE-FE) phase transition, in agreement with the earlier investigations on BFO bulk single-crystal and polycrystalline[6,30] samples. No evidence of soft phonon modes implies that the BFO has an order-disorder, first-order ferroelectric transition, unlike $PbTiO_3$. No decomposition of the BFO films was observed until 950 °C, suggesting that our film samples had few defects and dislocations. According to the experience of one of the authors (H.S.), bulk BFO is thermodynamically unstable in air without being in equilibrium contact with the Bi_2O_3/Fe_2O_3 flux. Since the decomposition is a first-order transition, it needs nucleation, and this is abundant in the case of the large surface of a very fine powder, starting to decompose at about 400 °C. This widely ignored fact was leading in the past, and is still leading to the preparation and description of impure powders or ceramic samples. The surface of single crystals, e.g., polished with a 1 μm diamond paste, proved to remain observable under the polarized light microscope up to the decomposition temperature (~933 °C). However, with increasing time, a multitude of dark spots developed on the surface, indicating nucleation of decomposition on polishing scratches [Fig. 8(c)]. It is expected that a defect-free surface of as-grown single crystals and of high quality films will withstand decomposition for a longer time.

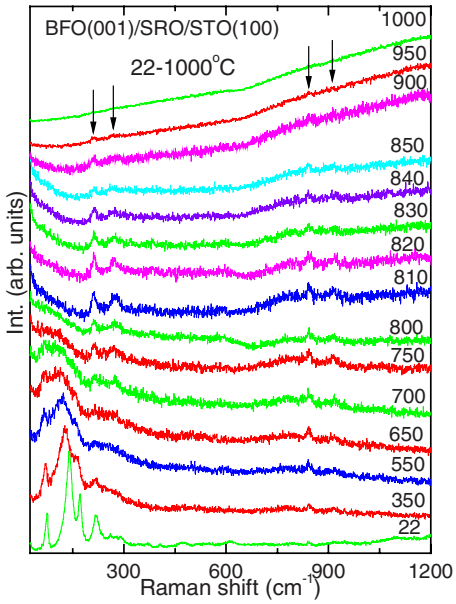

FIG. 4. (Color online) Temperature-dependent Raman spectra of (001)BFO thin film on SRO/STO substrates.

IV. RAMAN EFFECT IN β PHASE

The high-temperature Raman spectra (Fig. 4) show that four lines [~213, 272, 820, and 918 cm^{-1} (possibly second-order peak)] persist above the well known ferroelectric-phase transition temperature (820 °C). In the cubic perovskite phase, no first-order Raman lines are allowed because all the ions sit at the inversion centers and all long wavelength phonons are of odd parity. The data show that the β phase above 820 °C *cannot* be *cubic* as reported earlier.[30] Since our backscattering geometry with incidence radiation along the *Z* axis favors A_1 and B_1 phonons, four Raman modes ($3A_1+B_1$, normally silent) are predicted in the tetragonal (or orthorhombic) perovskite phase (Table I), in agreement with the experiment. Small orthorhombic splitting of four unob-

served E modes is predicted, but these modes are unobserved in the backscattering geometry. We observe no soft mode in these studies but merely some disappearance of several modes. The linewidth broadening and shifting toward low frequency at high temperature are compatible with the thermal expansion and disorder, suggesting that the α-β and β-γ transitions are both order-disorder, compatible with the eight-site model originally developed by Comes *et al.*[26] and developed in detail by Chaves *et al.*[29]

V. THERMODYNAMICS OF PHASES

The existence of a β phase below ~930 °C and below the decomposition point of $Bi_2Fe_4O_9$ at 960 °C has been known for some 40 years,[37] but the early Soviet work is rarely cited, and BFO was sometimes considered not to be a single-phase material. Using DTA in conjunction with high-temperature reflected polarized light microscopy, the Bi_2O_3-Fe_2O_3 phase diagram of Speranskaya *et al.*[37] has been strongly refined, mostly based on Ref. 16 and on x-ray results of the present work [Fig. 5(a)]. DTA thermograms shown in Fig. 5(b) illustrate the phase transformation sequence both for $BiFeO_3$ single crystals [small crushed dendrites (Fig. 1)] and target material of thin film.

The DTA [Fig. 5(b)] of crushed leaves of fernlike dendrites (Fig. 1) of BFO shows four sharp endothermic peaks at around 823, 925, 933, and 961 °C. They can be interpreted as (a) a first-order α-β transition, (b) a weakly first-order β-γ transition, (c) peritectic decomposition of the cubic phase into flux and $Bi_2Fe_4O_9$, and (d) the peritectic decomposition of $Bi_2Fe_4O_9$ into flux and Fe_2O_3. The phase transition temperatures obtained on powders of coarsely crushed single crystalline dendrites and polycrystalline target materials may be different for thin films, where transformations may be controlled by the built-up strain energy. These DTA data for $BiFeO_3$ and others for which the Bi/Fe ratio is varied with a view to determining the liquidus curves and the eutectic and peritectic horizontals, produce the phase diagram shown in Fig. 5(a). Since its first designation with the approximate composition $Bi_{40}Fe_2O_{63}$,[38] this Bi_2O_3-rich compound of the system was reported with slightly deviating compositions by different authors (e.g., $Bi_{46}Fe_2O_{72}$). We adopt now the formula $Bi_{25}FeO_{39}$ for the diagram, which is based on a thorough analysis of this sillenite structure,[39] showing that part of the Bi^{3+} is lodging on mixed site with Fe^{3+}, as expressed by $Bi_{12}(Bi^{3+}_{0.50}Fe^{3+}_{0.50})O_{19.5}$. We prefer that formula to $Bi_{25}FeO_{40}$,[40,41] which does not satisfy the charge balance. The recently published partial Bi_2O_3/Fe_2O_3 phase diagram,[41] based on DTA data, agrees partially with ours, but neither gives liquidus data nor shows the cubic phase. Moreover, the α- or β-phase transition temperature of Bi_2O_3 is also observed between "$Bi_{25}FeO_{40}$" and $BiFeO_3$, which appears to indicate nonequilibrium conditions.

High-temperature x-ray study of BFO powder (Fig. 6) showed that the rhombohedral bulk structure has a strongly first-order transition near 825(±5) °C to an orthorhombic structure. The unit-cell volume shrinks by more than 1% upon heating through this transition from 64.05 Å^3 (per formula unit) in the rhombohedral phase to 62.91 Å^3 in cubic

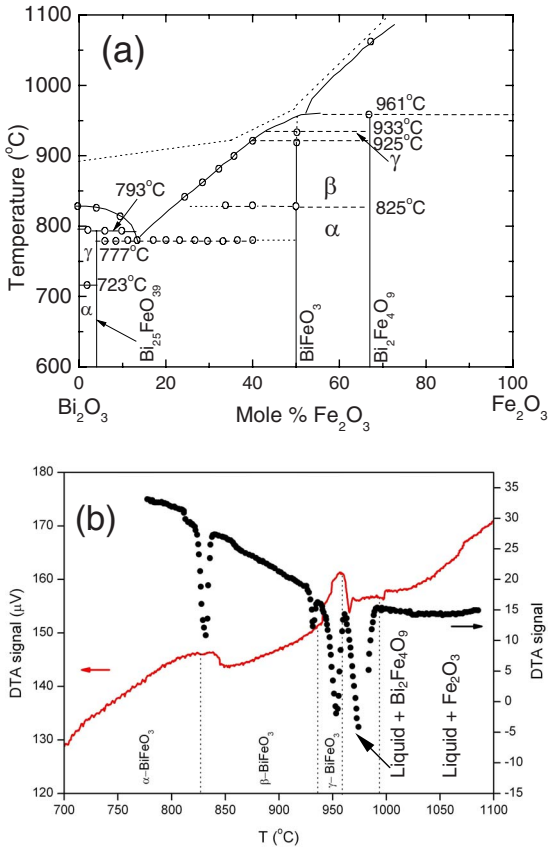

FIG. 5. (Color online) (a) Phase diagram of the Bi_2O_3-Fe_2O_3 system. Open circles show the data points obtained by DTA. The dotted line above the liquidus represents the approximate temperature limit not to be surpassed for avoiding decomposition, otherwise correct equilibrium DTA peaks are no longer observed upon a second heating. The α, β, and γ phases are rhombohedral, orthorhombic, and cubic, respectively. (b) DTA studies on crushed dendritic single crystal (dotted points) and target material of thin film (solid line) of $BiFeO_3$. Signal has been inverted and offset for clarity. Peak heights are proportional to the temperature difference between sample and reference.

phase. At around 925(±5) °C, there is a nearly second-order transition from an orthorhombic to a cubic $Pm\bar{3}m$ phase consistent with the disappearance of the β-phase ferroelastic domains and appearance of optical isotropy in polarized reflected light up to the decomposition temperature of 933(±5) °C. The orthorhombic and cubic phases have one formula group per unit cell. The rhombohedral cell parameter at 825 °C (in pseudocubic setting; in reality, there is a change of translation, see below) is a=4.0011 Å. The orthorhombic cell parameters at 825(±5) °C are a=3.9765(8) Å, b=3.9860(6) Å, and c=3.9687(8) Å; and at 905 °C are a=3.9892(13) Å, b=3.9926(9) Å, and c=3.9848(9) Å. In the cubic phase, a=3.9916(1) Å at around 925(±5) °C. The shortened bond length in the orthorhombic and cubic phases, compared with those in the rhombohedral phase, favors a metallic state. The existence of the metallic state above the magnetic ordered states implies that the metallic state is triggered by lattice contraction. Some oxide perovskites such as

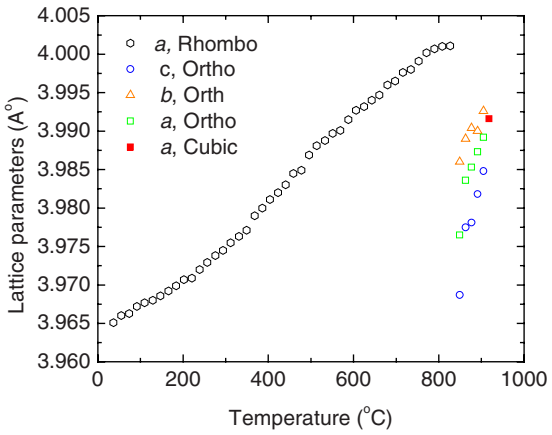

FIG. 6. (Color online) Temperature variation of lattice parameters for rhombohedral (pseudocubic setting), orthorhombic, and cubic phases of $BiFeO_3$. At 825 °C, the lattice constant a =4.0011 Å splits into a triplet (open circles, squares, and triangles), which combines again at about 925(±5) °C in the cubic phase (solid square), where a=3.9916 Å.

$NdNiO_3$ and related rare-earth nickelates show a sharp decrease of the unit-cell volume exactly at the metal-insulator transition.[42]

It is important to emphasize that the $BiFeO_3$ phase is thermodynamically metastable in air without contact of the equilibrium Bi_2O_3/Fe_2O_3 flux, a fact still widely ignored these days. It had been pinpointed in a critical review by Skinner[43] in 1970 that it was already shown in 1960 (Ref. 44) and 1961 (Ref. 45) that $BiFeO_3$ decomposes at around 700 °C irreversibly, and that "much of the discussion in the subsequent eight years with respect to the Curie point could have been avoided had suitable weight been given to these results." Ironically, this statement remains highly topical even nearly 50 years later after that statement. It was also shown shortly later by DTA[38,46] that $BiFeO_3$ is unstable in the vicinity of 800–850 °C and slowly decomposes. In the present work, this instability has been clearly shown by the visual observation of a multitude of decomposition dots all over the diamond-paste-polished surface of a single crystal in its β-phase state [Fig. 9(b)]. Since the decomposition reaction can be assimilated to a first-order transition, nucleation is required. Dislocations and other crystal defects are preferred places of nucleation. The speed of decomposition will depend on a variety of factors, such as temperature, exposure time at constant temperature, heating speed, the number of dislocations on the surface, ratio of surface to bulk volume, porosity and grain size of ceramics, etc. Thus, it can be expected that an as-grown single crystal with a smooth, dislocation-free brilliant surface will allow driving the temperature of decomposition of metastable $BiFeO_3$ in its cubic phase to still higher values than were observed in the present study. In the past, many erroneous results in studying $BiFeO_3$ were also caused by the coincidence of the melting temperature of $BiFeO_3$ with that of the α-β phase transition temperature. Another cause of errors, if ignored, may be the steep rise of vapor pressure of Bi_2O_3 above its melting point.[47] This will be lower in Bi_2O_3/Fe_2O_3 melts, but still not negligible and which may be the cause of irreversibility effects in heating-cooling experiments. For example, the observed irreversibility of DTA measuring points when the temperature was driven too high above the liquidus [see dotted critical line above liquidus in Fig. 5(a)] was probably caused by Bi_2O_3 loss. The possibility of pollution of furnaces and measuring setups by evaporated Bi_2O_3 should also be kept in mind. In summary, Skinner's statement "experimental measurements on $BiFeO_3$ and their interpretation are arduous and require the utmost skill and sophistication"[43] is keeping its full validity.

VI. SPACE GROUP OF PHASES: $BaTiO_3$ VERSUS $BiFeO_3$, A COMPARISON

The space groups of the $BaTiO_3$ phases are the following: $R3m/C_{3v}^5$, $Amm2/C_{2v}^{14}$, $P4mm/C_{2v}^1$, and $Pm\bar{3}m/O_h^1$,[48] and those of $BiFeO_3$ are $R3c/C_{3v}^6$, orthorhombic (possibly $P2mm/C_{2v}^{12}$, but a full space group analysis will be given elsewhere), and $Pm\bar{3}m/O_h^1$. Thus, only the cubic prototype phases have the same space group and a tetragonal phase is lacking in $BiFeO_3$. The polar groups of all three ferroelectric $BaTiO_3$ phases are maximal polar subgroups of $Pm\bar{3}m/O_h^1$, thus obeying "Ascher's maximal polar subgroup rule"[48] because all three phases are of the equitranslation type relative to the cubic prototype phase. In $BiFeO_3$, however, the rhombohedral space group $R3c$ is not a maximal polar subgroup, hence Ascher's rule is not followed. This is due to a nonequitranslation superstructure, consisting in an alternating twisting of the oxygen octahedrons around the polar axis, which results in a change of translations relative to the cubic prototype phase $Pm\bar{3}m$.[8,33,49] If a phase transition is accompanied by a change of translation (here relative to the prototype phase), then the formation of antiphase domains in the ferroic phase is always allowed.[50] The recent observation of antiphase domains in $BiFeO_3$ films, using x-ray diffraction,[51] is in agreement with the nonequitranslation character of the rhombohedral phase. More detailed studies of the antiphase domains in single crystals will be rewarding. The study of their etched walls by observation under the optical microscope, by x-ray techniques, and by electron microscopy are well established methods (cf., e.g., Refs. 52 and 53). It is conjectured that cycling the crystal through the α-β first-order transition, as well as ferroelectric switching, will greatly increase the number of antiphase domains and their walls.

VII. DOMAIN STRUCTURES IN $BiFeO_3$ SINGLE CRYSTAL

The Raman spectra do not discriminate between orthorhombic and tetragonal structures for the β phase, but domain structures do, in particular, when viewed in transmitted polarized light. Ferroelastic domains of the rhombohedral α phase of BFO have repeatedly been studied by polarized light microscopy, by transmission and reflection in Ref. 16, by transmission alone in Refs. 54–56, and by reflection alone in Refs. 8, 14, 17, 49, and 57. Because of the strong absorbance of BFO,[56] studies in transmission are possible below

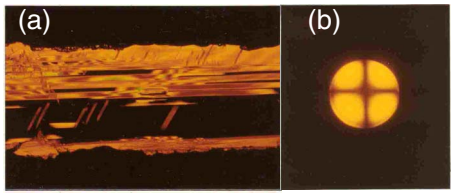

FIG. 7. (Color online) $BiFeO_3$ (111)pc cut in transmission with crossed polarizers, thickness about 9 μm. (a) Orthoscopy; black isotropic stripe in middle with P_s perpendicular to plane. (b) Uniaxial conoscopy figure with crossed polarizers of black stripe in (a) between the two clear ones, with P_s inclined at 34° 16′ with respect to the surface. The length of the part of the crystal plate shown is ~3 mm.

about 30 μm thickness only and at temperatures not higher than about 600 °C, because of the strong shift of the absorption edge to the red with increasing temperature. Thanks to an extremely high birefringence of rhombohedral BFO (Δn =0.34 at λ=550 nm in the principal section),[55] excellent contrast between ferroelastic domains was obtained down to about 9 μm thickness, the lowest thickness achieved by polishing. Even for that very thin wafer, a good conoscopic figure was obtained (Fig. 7). For thick samples and high temperatures, observation in reflected polarized light is obligatory. In reflected light, less information can be obtained than in transmission, because only the traces of the ferroelastic domain walls can be seen, not the walls' inclination relative to the surface. The reflectivities and bireflectance values of α-BFO have so far not yet been quantitatively characterized, as this has been done, e.g., for $YBa_2Cu_3O_{7+\delta}$.[57,58] Such a characterization would greatly facilitate work with single crystals and their ferroelastic domains. As an example of the contrast which can be obtained between ferroelastic domains with the principal reflectance in the plane, we show a cross section through a leaf of the fernlike dendrites (Fig. 8).

The α phase of BFO forms pseudocubic (pc) (100)pc and (110)pc walls, the orientation and appearance of which in transmission on (100)pc, (110)pc, and (111)pc cuts have been represented schematically in detail in Fig. 13 of Ref. 59. Whereas an orthorhombic phase of a perovskite with two lattice parameters parallel to ⟨110⟩pc directions and one parallel to ⟨100⟩pc also forms (100)pc and (110)pc walls [in the case of orthorhombic $BaTiO_3$, corresponding to Aizu species[60] No. 689, $m\bar{3}m1'Fmm21'(ss)$], the orthorhombic phase determined for BFO in this work has all three lattice parameters parallel to ⟨100⟩pc directions, corresponding to Aizu species No. 688, $m3m1'Fmm21'(pp)$. Only (110)pc walls are expected for this phase, as is the case for a tetragonal perovskite phase. Thus, here we encounter the same problem as with the Raman effect, that no easy discrimination is possible between tetragonal and orthorhombic phases in reflected light if only traces of walls can be taken into account and not exact reflectance values and orientations. However, the observed tripling of the pseudocubic lattice parameter excludes a tetragonal phase, which should show a doubling only with intensity ratio 2:1 of the lines, with "1" for the polar direction. For the orientation of the orthorhombic cell as in $BaTiO_3$, discrimination is possible, because in that case, in addition to (110)pc walls, also (100)pc walls are allowed as in the rhombohedral case. [For both orthorhombic species, 6 ferroelastic and 12 ferroelectric domain states are possible. For the rhombohedral α phase (species No. 753, $m\bar{3}m1'F3m1'$), four ferroelastic and eight ferroelectric domain states are allowed.] In Fig. 9, we see that the β-BFO phase has been recognized on a (111)pc cut to be ferroelastic and *noncubic* on the basis of rectilinear traces of ferroelastic walls and a clear α-β phase boundary [Fig. 9(c)]. Nearly exclusively, traces of (110)pc walls can be seen, consistent with the x-ray results, i.e., orientation of the three orthorhombic axes parallel to ⟨100⟩pc. In some tiny regions, also lines perpendicular to the former ones can be seen (difficult to see in print), which are due to (100)pc walls. If these small regions would really belong to the β phase, the orthorhombic cell orientation of the $BaTiO_3$ type or rhombohedral symmetry would be possible. However, since the photo was taken very close to the transition temperature, the small regions represent probably remainders of untransformed α phase. The observed splitting into a triplet of pseudocubic lattice parameters also excludes rhombohedral symmetry and disagrees entirely with the rhombohedral space group $R3m$, claimed for the β phase at 824 °C.[41] When observing a (100)pc surface in the β-phase temperature range in reflected polarized light, the occurrence of extinction with crossed po-

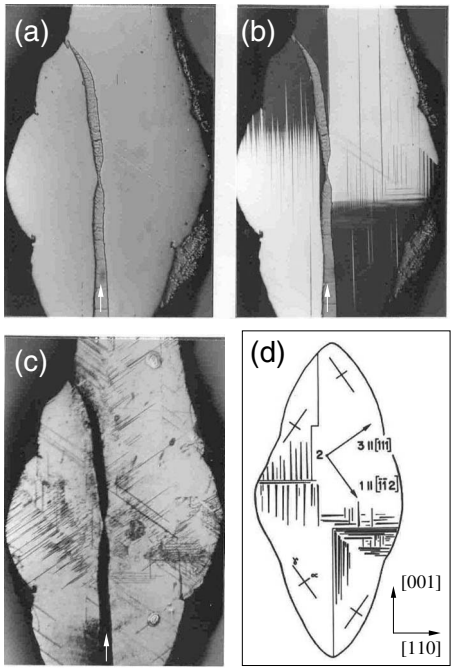

FIG. 8. Cross section through a leaf of dendrite, parallel to a (110)pc plane: polished surface (a) in unpolarized light and (b) with crossed polarizers for two domains with P_s in plane. (c) After etching, sharp spikes point in the direction of P_s. (d) Schematic; the crosses corresponding to the black and white domain fields in (b) represent the orientation of the principal section of the reflectivity ovaloid (principal bireflectance=$R_\gamma - R_\alpha$). The approximately vertical, thick, irregular trace (indicated with white arrow), visible in (a)–(c), represents an inclusion of flux. The horizontal extension of the crystal's cross section is ~2.5 mm.

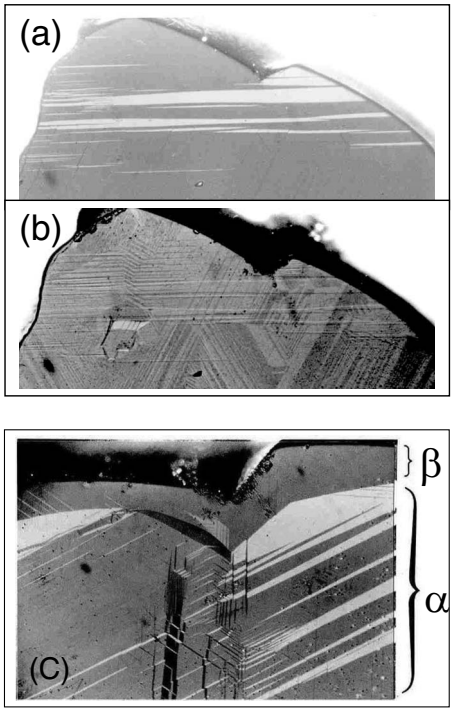

FIG. 9. Evolution of domain structure in polished pseudocubic (111)pc cut of dendritic BFO single crystal (Fig. 1) (Ref. 16) at different temperatures: (a) at 27 °C, ferroelastic domains of α phase, separated by traces of (110)pc walls. Reflected, polarized light, dark domains in extinction position; nearly crossed polarizers (for contrast formation in reflection, consult Ref. 57. (b) At 820 °C, ferroelastic domains of β phase; majority of rectilinear traces due to (110)pc walls. A few lines, perpendicular to the former ones, are due to traces of (100)pc walls. Specular reflection with polarizer only; contrast due to puckered surface. Small dark dots indicate nuclei of starting decomposition. (c) At 820 °C, showing the coexistence of α and β phases, separated by a sharp first-order phase boundary. The horizontal extension of the visible part of the crystal is ~3 mm.

larizers along ⟨110⟩pc directions in certain domains, besides other domains with extinction parallel to ⟨100⟩pc, would clearly indicate the $BaTiO_3$-type orientation of the orthorhombic unit cell with P_s along a ⟨110⟩pc direction. Such a test has not been made so far.

The postulation of a cubic γ phase in a very narrow temperature interval was initially based on the reflected polarized light observation that the ferroelastic domains of the β phase disappear at about 925 °C, leaving the sample optically isotropic up to the decomposition point of the cubic BFO phase at 933 °C. At these high temperatures, the strong red light scattering of the furnace did not allow taking a good photograph.

The ferroelastic nature of the α-β phase transition is necessary and sufficient to satisfy the Toledano[61] requirement that changes in crystal class are required for ferroelastic transitions (this treats rhombohedral and trigonal phases as a single superclass). Thus, for example, the monoclinic-monoclinic $C_{2h}-C_2$ transition of triglycine sulphate cannot be ferroelastic, but is of the *coelastic* type.[62]

The primary purpose of the section above is to establish the main properties of the β phase and show that it cannot be tetragonal; we cannot rule out a small monoclinic distortion, but we see no evidence of that in our data, which appear orthorhombic. The data of Kornev *et al.*[63] suggest monoclinic, but their monoclinic angle is 90° within their quoted uncertainty (two standard deviations). We are skeptical of this because monoclinic-cubic transitions are extremely unusual in nature, and this would be odd or even unique.

VIII. γ PHASE

BFO single crystals have dark-gray metallic luster and are yellow-brown in transmission below about 30 μm thickness. Upon heating, they turn to deep red before getting opaque at about 700 °C.[56] The band gap of BFO is calculated to be E_g=2.8 eV,[64] and usually measured experimentally as 2.5 eV. However, there is a large band-gap shift at the α-β phase transition temperature. If we define the band edge as where the absorption is 100 at 10 μm, then the experimental gaps are 2.25, 2.18, 2.00, and 1.69 eV at 20, 160, and 300 °C, respectively. However, it shifts abruptly to 1.5 eV at 550 °C, above which the E_g values are not yet known. There has been some controversy about its leakage current, with Clark and Robertson[64] showing that the ambient band gap is too large for intrinsic mechanisms. Optical absorption measurement [Fig. 10(a)] shows that the band gap decreases slowly and linearly with temperature in the α and β phases, from 2.5 eV to about 1.5 eV, but then drops abruptly to near zero at the β-γ transition near 925 °C. Our observation is, thus, that E_g decreases significantly by the α-β transition temperature, and hence, conduction in the high-temperature β phase can be intrinsic. The cubic γ phase is opaque. That is compatible with our band structure calculations (following section) that a noncubic distortion is required to give it a finite band gap. Thus, we regard β-BFO phase as semiconducting with small gap (calculated ~1.5 eV) and γ-BFO phase from ~930 to ~960 °C as cubic and metallic; above 960 °C, decomposition occurs. Note that some Bi-containing oxide perovskites such as $Ba(_{0.6})K(_{0.4})BiO_3$ (Refs. 65 and 66) also show insulator-metal transition and become cubic upon entering into the metallic state. This compound has a rather quite different electronic structure compared to the BFO and has Bi ion at the B site, whereas it is at the A site in $BiFeO_3$. However, this compound has a common antiferromagnetic ordering with $BiFeO_3$. The data graphed in Fig. 10(a) were obtained in two different ways: by conventional absorption spectroscopy at a fixed temperature; and with fixed wavelength (632.8 nm He-Ne) by slowly varying temperature and using the Urbach equation to relate absorption coefficient (a) to band gap $E_g(T)$: $\log a(T)=(E-E_g)/E_g$ +constant. We infer that the band gap could follow the "dotted" line drawn in Fig. 10(a). However, experiment with different laser lines of fixed wavelength would be useful to study the exact nature of the band-gap variation at high temperature. The reflective measurement [Fig. 10(b)] on BFO thin film on STO substrate shows a sudden increase in reflectivity (metallic behavior) above 900 °C. In addition, the surface of the single-crystal samples was observed visually in both the He-Ne transmission and in diamond anvil pressure studies, to be reported separately; at the cubic metal-

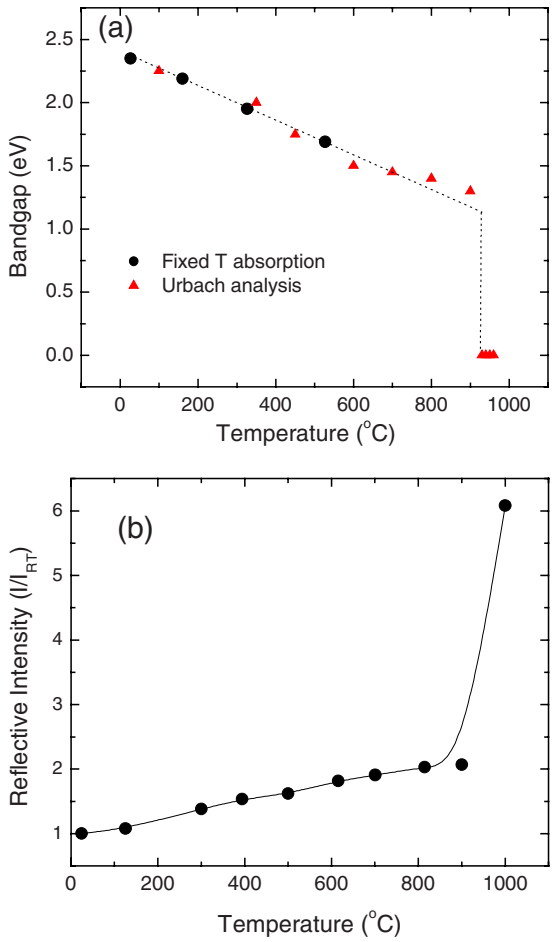

FIG. 10. (Color online) Band-gap energy in $BiFeO_3$ from room temperature to its peritectic decomposition point. The data show a linear decrease from about 2.5 eV at ambient temperature to about 1.5 eV at 550 °C, followed by a discontinuous drop at the β-γ transition near zero (metallic). For the lower-temperature data points, the gap is arbitrarily assigned as the energy (wavelength) at which the absorption exceeds 100 cm^{-1}; this is probably about 0.15 eV below the true band gap. The broken (dotted) line was drawn to infer the nature of band-gap change. (b) Temperature vs reflective intensity of BFO thin film. The intensity was normalized to its room-temperature intensity (I_{RT}) and the wavelength used was 514.5 nm.

insulator transition, the surface suddenly becomes highly reflecting (metallic). This process is reversible upon heating or cooling, and does not signify melting.

IX. ELECTRICAL CONDUCTIVITY

Figure 11 shows high-temperature dc resistivity measurements on a small single crystal. The resistivity was found to decrease from $>10^{10}$ Ω cm at room temperature to 50 Ω cm at the temperature of the β-γ transition. The conductivity band gap was not constant, decreasing from ~1.3 eV to ~0.6 eV with increasing temperature. This is much smaller than the optical band gap, and lies in the near infrared region; since the single crystal is very dark, a substantial optical absorption can be understood. The resistivity as a function of temperature shows a change of slope from negative to positive around 920 °C (Fig. 11) which we interpret as an indication of the metal-insulator (M-I) transition, although we note that the positive slope is anomalously high for a normal metal. The change of slope is at a temperature close to, but lower than, the decomposition temperature. On the other hand, positive temperature coefficients of resistivity due to barrier layers have been measured near the paraelectric transitions of semiconductor ferroelectrics[67] although we notice that in that case one should expect the anomaly to be larger in ceramics than in single crystals. The anomaly was also seen in ceramics[68] but it was quantitatively and qualitatively identical to that of crystals, suggesting that it is not due to a barrier effect but to a real M-I transition.

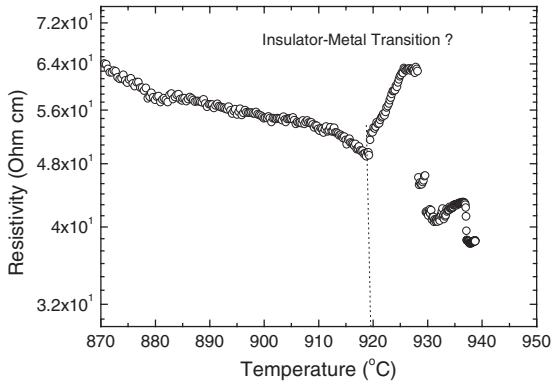

FIG. 11. Two-point resistance measurement $R(T)$ of $BiFeO_3$ single crystal. The resistance drops by 10^9 between 20 °C and about 920 °C in this sample. We interpret the change in sign of dR/dT at 920 °C as from semiconducting (negative) to metallic (positive). The discontinuity at about 930–940 °C in this sample is presumably phase decomposition. The few degrees difference between the apparent metal-insulator transition in this specimen and that in Fig. 10 may be the different morphology of the sample, which is a bulk single crystal rather than a strained film.

X. BAND STRUCTURE MODEL: BAND-GAP COLLAPSE AND METAL-INSULATOR TRANSITION

Obtaining a band gap of zero is a common artifact in theoretical models using the local density approximation. Therefore, in the present study, we circumvent this by using the screened exchange method.[69] This method is a density functional method based on Hartree-Fock, which includes the electron exchange via a Thomas-Fermi screened exchange term. It gives the correct band gap of many oxides, including antiferromagnetic NiO and rhombohedral $BiFeO_3$.[64] We find that the band gap of the cubic phase of BFO is indeed zero, as shown in Fig. 12(a). The Fermi level lies within the Fe 3*d* states. It is interesting that in the cubic phase there is a direct gap at any point in the zone, and this opens up into a true band gap of 0.8 eV (calculated) in the orthorhombic phase as seen in Fig. 12(b). Note that at RT the BFO has an indirect band gap, but the direct gap lies only about 0.05 eV above it, and the valence band is very flat. Thus, with increasing T, as the conduction band descends, the gap can become direct.

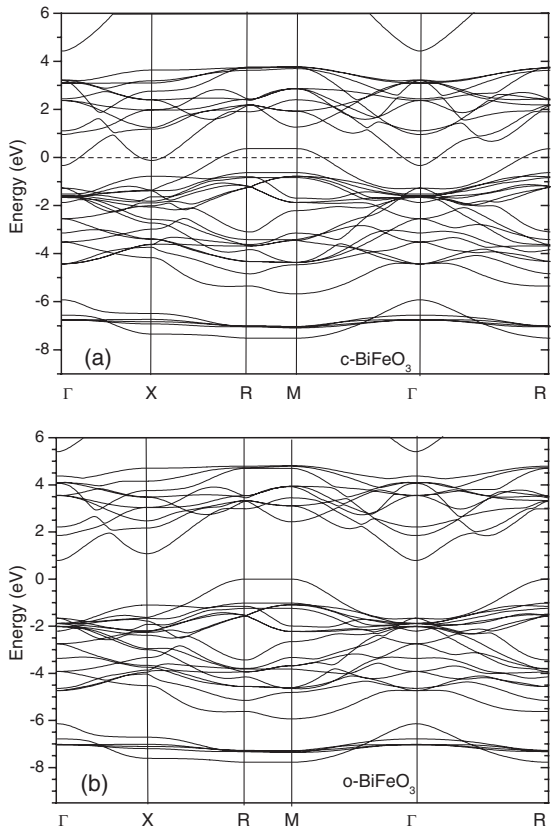

FIG. 12. Band-gap energy calculation for $BiFeO_3$ using screened exchange method for different structures: (a) cubic and (b) orthorhombic. Fermi level is at 0 eV in (a), and the valence band maximum is at 0 eV in (b).

We find (to be published separately) that the same cubic phase of $BiFeO_3$, as is measured at atmospheric pressure at 931 °C, is also reached at room temperature and at hydrostatic pressure of about 47 GPa. It is already known that magnetism also disappears at 47 GPa.[70] Those authors suggested a metal-insulator transition as one of three hypotheses for their Mossbauer data. Thus, both the present resistance data and the high-pressure data support the metal-insulator transition interpretation.

The differences in transition temperatures between bulk and thin film, and single crystal, and also between the different studies drawn together in this paper, show that the transitions in the thin film are at higher temperatures than in the bulk material. The effect of pressure on these sorts of transitions is known; they have a negative dp/dT slope, as pressure stabilizes the higher symmetry phases in $BaTiO_3$. The thin film data would be consistent with this if you regard any surface relaxation or epitaxial strains in the thin films as imposing a negative pressure or lower density on the thin films. The large negative change in volume observed at the rhombohedral-orthorhombic transition in BFO is also consistent with the transition having a strong negative Clapeyron slope, so surface relaxation might be expected to move the transition to higher temperature in the thin film.

XI. CONCLUSION

In conclusion, high quality epitaxial (001)BFO films have been grown on (100)STO substrates using PLD. The x-ray diffraction (XRD) studies showed that films are *c*-axis oriented with high degree of crystallinity. The RT polarized Raman scattering of (001)BFO films showed monoclinic symmetry, in agreement with synchrotron studies. The results obtained from DTA, high-temperature XRD, optical absorption and reflectivity, and reflected polarized light microscopy studies of domains were consistent. A refinement of the Bi_2O_3-Fe_2O_3 phase diagram has been undertaken. We observed the FE-FE α-β structural phase transition at around 820 °C; no softening of Raman modes was observed at low frequencies. An intermediate β-$BiFeO_3$ phase between 820 and 925(±5) °C has been observed and recognized to be orthorhombic. The existence of the cubic gamma phase has been established between 925 (±5) and 933 (±5) °C by combining reflected polarized light microscopy, DTA on crushed single crystals, x-ray, and electric conductivity measurements. The sequence of phases is monoclinic-orthorhombic-cubic in film and rhombohedral-orthorhombic-cubic in bulk; the rhombohedral and orthorhombic phases of $BiFeO_3$ differ notably from those in $BaTiO_3$. Moreover, the transitions appear to be order-disorder from the Raman data, suggesting that the eight-site model of Comes *et al.*[26] and Chaves *et al.*[29] is applicable. The existence of the metal-insulator transition is consistent with dc conductivity measurement, optical absorption and reflectivity, high-pressure studies, and band structure model.

ACKNOWLEDGMENTS

We thank W. Perez, M. K. Singh, and S. R. Das for experimental help, and M. Alexe, B. Dkhil, and J. Kreisel for sharing their unpublished results. This work was supported by the DoD W911NF-06-0030 and W911NF-05-1-0340 grants and by a EU-funded project "Multiceral" (NMP3-CT-2006-032616) at Cambridge. H.S. and P.T. thank the Swiss NSF for support and Hélène Lartigue for help in DTA of dendritic single crystals.

[1] H. Schmid, Ferroelectrics **162**, 317 (1994).
[2] J. Wang, J. B. Neaton, H. Zheng, V. Nagarajan, S. B. Ogale, B. Liu, D. Viehland, V. Vaithyanathan, D. G. Schlom, U. V. Waghmare, N. A. Spaldin, K. M. Rabe, M. Wuttig, and R. Ramesh, Science **299**, 1719 (2003).
[3] M. Fiebig, T. Lottermoser, D. Fröhlich, A. V. Goltsev, and R. V. Pisarev, Nature (London) **419**, 818 (2002).
[4] Y. Tokura, Science **312**, 1481 (2006).
[5] N. A. Hill, J. Phys. Chem. B **104**, 6694 (2000).
[6] P. Fischer, M. Polomska, I. Sosnowska, and M. Szymański, J.

Phys. C **13**, 1931 (1980).
[7] G. A. Smolenskii and I. Chupis, Sov. Phys. Usp. **25**, 475 (1982).
[8] F. Kubel and H. Schmid, Acta Crystallogr., Sect. B: Struct. Sci. **46**, 698 (1990).
[9] I. Sosnowska, T. Peterlin-Neumaier, and E. Steichele, J. Phys. C **15**, 4815 (1982).
[10] C. Tabares-Munoz, J. F. Rivera, A. Bezinges, A. Monnier, and H. Schmid, Jpn. J. Appl. Phys., Part 1 **24**, 1051 (1985).
[11] J. D. Bucci, B. K. Robertson, and W. J. James, J. Appl. Crystallogr. **5**, 187 (1972).
[12] A. Palewicz, R. Przeniosto, I. Sosnowska, and A. W. Hewat, Acta Crystallogr., Sect. B: Struct. Sci. **63**, 537 (2007).
[13] V. V. Shvartsman, W. Kleemann, R. Haumont, and J. Krisel, Appl. Phys. Lett. **90**, 172115 (2007).
[14] D. Lebeugle, D. Colson, A. Forget, M. Viret, P. Bonville, J. F. Marucco, and S. Fusil, Phys. Rev. B **76**, 024116 (2007).
[15] D. Lebeugle, D. Colson, A. Forget, and M. Viret, Appl. Phys. Lett. **91**, 022907 (2007).
[16] C. Tabares-Muñoz, Ph.D. thesis, University of Geneva, Switzerland, 1986.
[17] F. Kubel and H. Schmid, J. Cryst. Growth **129**, 515 (1993).
[18] J. Li, J. Wang, M. Wuttig, R. Ramesh, N. Wang, B. Ruette, A. P. Pyatakov, A. K. Zvezdin, and D. Viehlanda, Appl. Phys. Lett. **84**, 5261 (2004).
[19] R. R. Das, D. M. Kim, S. H. Baek, C. B. Eom, F. Zavaliche, S. Y. Yang, R. Ramesh, Y. B. Chen, X. Q. Pan, X. Ke, M. S. Rzchowski, and S. K. Streiffer, Appl. Phys. Lett. **88**, 242904 (2004).
[20] K. Y. Yun, D. Ricinschi, T. Kanashima, and M. Okuyama, Appl. Phys. Lett. **89**, 192902 (2006).
[21] C. Ederer and N. A. Spaldin, Phys. Rev. B **71**, 224103 (2005).
[22] W. Eerenstein, F. D. Morrison, J. Dho, M. G. Blamire, J. F. Scott, and N. D. Mathur, Science **307**, 1203a (2005).
[23] M. K. Singh, S. Ryu, and H. M. Jang, Phys. Rev. B **72**, 132101 (2005).
[24] X. Qi, J. Dho, R. Tomov, M. G. Blamire, and J. L. MacManus-Driscoll, Appl. Phys. Lett. **86**, 062903 (2005).
[25] G. Xu, H. Hiraka, G. Shirane, J. Li, J. Wang, and D. Viehland, Appl. Phys. Lett. **86**, 182905 (2005).
[26] R. Comes, M. Lambert, and A. Guinier, Solid State Commun. **6**, 715 (1968).
[27] J. F. Scott, Phys. Rev. **183**, 823 (1969).
[28] S. Geller and P. M. Raccah, Phys. Rev. B **2**, 1167 (1970).
[29] A. S. Chaves, F. C. S. Barreto, R. A. Nogueira, and B. Zēks, Phys. Rev. B **13**, 207 (1976).
[30] R. Haumont, J. Kreisel, P. Bouvier, and F. Hippert, Phys. Rev. B **73**, 132101 (2006).
[31] R. Blinc (private communication).
[32] H. J. Scheel and E. O. Schulz-Dubois, J. Cryst. Growth **8**, 304 (1971).
[33] C. Ederer and N. A. Spaldin, Phys. Rev. B **71**, 060401(R) (2005).
[34] R. Palai, H. Schmid, and R. S. Katiyar (unpublished).
[35] H. Schmid, Int. J. Magn. **4**, 337 (1973).
[36] S. J. Joshua, *Symmetry Principles and Magnetic Symmetry in Solid State Physics* (Hilger, Bristol, 1991), Appendix G.
[37] E. I. Speranskaya, V. M. Skorikov, E. Y. Rode, and V. A. Terekhova, Bull. Acad. Sci. USSR, Div. Chem. Sci. (English Translation) **5**, 874 (1965).
[38] P. Royan and K. Swars, Angew. Chem. **69**, 779 (1957).
[39] S. F. Radaev, L. A. Muradyan, and V. I. Simonov, Acta Crystallogr., Sect. B: Struct. Sci. **47**, 1 (1991).
[40] D. C. Craig and N. C. Stephenson, J. Solid State Chem. **15**, 1 (1975).
[41] A. Maītre, M. Franēois, and J. C. Gachon, J. Phase Equilibria and Diffusion **25**, 59 (2004).
[42] J. L. García-Muñoz, J. Rodríguez-Carvajal, P. Lacorre, and J. B. Torrance, Phys. Rev. B **46**, 4414 (1992).
[43] S. M. Skinner, IEEE Trans. on Parts, Materials, and Packaging **6**, 68 (1970).
[44] V. S. Filip'ev, N. P. Smolyaniov, E. G. Fesenko, and I. N. Belyaev, Sov. Phys. Crystallogr. **5**, 916 (1960).
[45] S. A. Fedulov, Yu. N. Venevtsev, G. S. Zhdanov, and E. G. Smazhevskaya, Sov. Phys. Crystallogr. **6**, 640 (1961).
[46] E. I. Speranskaya, V. M. Skorikov, E. Ya. Rode, and V. A. Terekhova, Bull. Akad. Sci. USSR, Chem. Ser. **15**, 873 (1965).
[47] V. K. Il'in, Russ. J. Inorg. Chem. **21**, 899 (1976); Zh. Neorg. Khim. **21**, 1645 (1976).
[48] E. Ascher, Phys. Lett. **20**, 352 (1966).
[49] F. Kubel, Z. Kristallogr. **210**, 5 (1995).
[50] H. Wondratschek and W. Jeitschko, Acta Crystallogr., Sect. A: Cryst. Phys., Diffr., Theor. Gen. Crystallogr. **32**, 664 (1976).
[51] L. Wana, Y. Lib, X. Mengb, J. Sunb, X. Yuana, J. Shangguana, and J. Chu, Physica B **391**, 124 (2007).
[52] B. Capelle and C. Malgrange, J. Appl. Phys. **53**, 6762 (1982).
[53] B. Capelle and C. Malgrange, J. Phys. (Paris) **45**, 1827 (1984).
[54] A. Steiner, C. Tabares-Muñoz, and H. Schmid, Helv. Phys. Acta **60**, 294 (1987).
[55] J. P. Rivera and H. Schmid, Ferroelectrics **55**, 23 (1997).
[56] C. Tabares-Muñoz, J. P. Rivera, and H. Schmid, Ferroelectrics **55**, 235 (1984).
[57] H. Schmid, E. Burkhardt, E. Walker, W. Brixel, M. Clin, J.-P. Rivera, J.-L. Jorda, M. Francois, and K. Yvon, Z. Phys. B: Condens. Matter **72**, 305 (1988).
[58] H. Rabe, J. P. Rivera, E. Burkhardt, and H. Schmid, Scientific and Technical Information **X**, 174 (1993).
[59] H. Schmid, Phys. Status Solidi **37**, 209 (1970).
[60] K. Aizu, Phys. Rev. B **2**, 754 (1970).
[61] J. C. Toledano, Phys. Rev. B **12**, 943 (1975).
[62] E. H. K. Salje, *Phase Transition in Ferroelastic and Co-elastic Crystals* (Cambridge University Press, Cambridge, England, 1990).
[63] I. A. Kornev, S. Lisenkov, R. Haumont, B Dkhil, and L. Bellaiche, Phys. Rev. Lett. **99**, 227602 (2007).
[64] S. J. Clark and J. Robertson, Appl. Phys. Lett. **90**, 132903 (2007).
[65] R. J. Cava, B. Batlogg, J. J. Krajewski, R. Farrow, L. W. Rupp Jr., A. E. Whatite, K. Short, W. F. Peck, and T. Kometani, Nature (London) **332**, 814 (1988).
[66] S. Tajima, M. Yoshida, N. Koshizuka, H. Sato, and S. Uchida, Phys. Rev. B **46**, 1232 (1992).
[67] J. Goodman, J. Am. Ceram. Soc. **46**, 48 (1963);W. Heywang, *ibid.* **47**, 484 (1964).
[68] M. Alexe (private communication).
[69] J. Robertson, K. Xiong, and S. J. Clark, Phys. Status Solidi B **243**, 2054 (2006).
[70] A. G. Gavriliuk, V. V. Struzhkin, I. S. Lyubutin, M. Y. Hu, and H. K. Mao, JETP Lett. **82**, 224 (2005).